ELSEVIER

Journal of Physics and Chemistry of Solids 63 (2002) 1993–2001

JOURNAL OF PHYSICS AND CHEMISTRY OF SOLIDS

www.elsevier.com/locate/jpcs

Defects and impurities in nanodiamonds: EPR, NMR and TEM study

A.I. Shames[a,*], A.M. Panich[a], W. Kempiński[b], A.E. Alexenskii[c], M.V. Baidakova[c], A.T. Dideikin[c], V.Yu. Osipov[c], V.I. Siklitski[c], E. Osawa[d], M. Ozawa[d], A.Ya. Vul'[d,1]

[a]*Department of Physics, Ben-Gurion University of the Negev, P.O. Box 653, 84 105 Be'er-Sheva, Israel*
[b]*Institute of Molecular Physics, Polish Academy of Sciences, Smoluchowskiego 17, 60-179 Poznań, Poland*
[c]*Ioffe Physico-Technical Institute, 26 Polytechnicheskaya, St Petersburg 194021, Russian Federation*
[d]*Toyohashi University of Technology, Toyohashi, Japan*

Received 9 October 2001; revised 4 February 2002; accepted 5 February 2002

Abstract

EPR, ^{13}C NMR and TEM study of ultradisperse diamond (UDD) samples is reported. The compounds show a high concentration of paramagnetic centers (up to 10^{20} spin/g), which are due to structural defects (dangling C–C bonds) on the diamond cluster surface. The anomalous reduction in the spin–lattice relaxation time of ^{13}C (from several hours in natural diamond to ~150 ms in UDD clusters) is attributed to the interaction between the unpaired electrons of the paramagnetic centers and nuclear spins. ^{13}C NMR line-width reflects the fact that the structure of the UDD surface is distorted in comparison to the 'bulk' diamond structure.

Keywords: D. Electron paramagnetic resonance (EPR); D. Nuclear magnetic resonance (NMR)

1. Introduction

Nanodiamond, often called ultradisperse diamond (UDD), is one of the new carbon cluster substances that may be produced in large amounts by the detonation method [1,2]. The study of UDD properties was initiated in 1988, with the focus on its technology and mechanical properties. An unusual feature of UDD is the small size of clusters, with most particles varying between 40 and 50 Å [3–6]. UDD is attractive for use as a polishing material and for seeding treatment of the substrate in CVD diamond film growth [7]. UDD powder can also be used as a starting material to produce onion-like carbon by heat treatment [8,9]. Besides, UDD may serve as a suitable model material for the investigation of phase transformations in carbon clusters. The latter idea is based on (i) the observation that onion-like carbon may be transformed to diamond by an electron beam [10] and by low temperature treatment [11] and (ii) the assumption that diamond, rather than graphite, is a thermodynamically stable form of carbon in a small cluster [12,13].

We have recently shown that a UDD cluster has a complex structure consisting of a diamond core of about 45 Å in size and a shell made up of sp^2-coordinated carbon atoms. We used X-ray diffraction and small angle X-ray scattering to answer the question as to how the shell structure and thickness vary with the explosion conditions and chemical purification of UDD clusters from the soot produced by the detonation process [14,15]. We found the shell to be strongly dependent on the earlier technological parameters.

A specific feature of clusters as nanosized objects is the crucial effect of the surface on their structural and electronic properties, since the number of surface atoms becomes comparable with that of bulk atoms. In this connection, it is important to understand the structural differences between defect centers in nanodiamond and those in bulk diamond. Where are impurities and defects localized? May size effects be detected in ultra-disperse diamonds? What are the parameters of defects and impurities in UDD? In this paper, we present the results obtained by EPR, NMR and TEM techniques, which may provide answers to these questions.

* Corresponding author. Fax: +972-8-6472904.
E-mail address: sham@bgumail.bgu.ac.il (A.I. Shames).
[1] Permanent address: Ioffe Physico-Technical Institute, St Petersburg, Russian Federation.

0022-3697/02/$ - see front matter
PII: S0022-3697(02)00185-3

Table 1
UDD samples description and conditions of chemical treatment

Sample number	Type of synthesis	Conditions of chemical treatment
#1 'Detonation carbon'	Dry	Without any chemical treatment
#2	Dry	HNO_3 50%, 200 °C
#4	Dry	HNO_3 50%, 210 °C
#3	Dry	HNO_3 50%, 230 °C
#5	Wet	HNO_3 50%, 210 °C
#6	Dry	HNO_3 70%, 250 °C

2. Experimental

The experiments were carried out on UDD samples extracted from carbon black soot ('detonation carbon') produced by the detonation of explosives containing excess carbon, namely, a mixture of TNT and hexogene (TNT/hexogene = 60/40) [1]. The UDD samples were obtained by 'dry-and-wet' synthesis [14], in which the detonation products were cooled by a gas and water.

The diamond phase was extracted by treating the carbon soot with nitric acid in an autoclave. The degree of removal of the non-diamond phase was controlled by the treatment temperature. After the reaction was completed and the material was removed from the autoclave, it was treated with distilled water until pH = 7 was reached. The UDD samples prepared in this way were identical in all parameters, except the amount of the amorphous phase surrounding the diamond core. The parameters of the oxidation processes are listed in Table 1.

Room temperature (RT, $T = 297$ K) EPR spectra were registered using a Bruker EMX-220 digital X-band (9.4 GHz) spectrometer. They were taken at non-saturating microwave power of 200 μW and 100 kHz magnetic field modulation of 0.2 and 0.02 mT. Signal saturation measurements were made within the incident power range from 2 μW to 200 mW. The g-factors and concentrations were determined precisely by a simultaneous recording of the sample under study and 1.1×10^{-3} M TEMPOL solution in ethanol ($g = 2.0059 \pm 0.0001$). The g-factors were found from the minima in the second derivative of the EPR spectra. Low temperature X-band EPR measurements were made using a Radiopan ES/X spectrometer equipped with an Oxford Instruments gas flow helium cryostat within the temperature range 4.2–300 K. The microwave frequency was measured by a microwave frequency counter with an accuracy of 5 kHz. The magnetic field was calibrated by a JTM-147 tracking NMR magnetometer within the accuracy of 0.005 mT. The EPR spectra processing (digital filtering, differentiation, baseline correction, and numerical integration) was performed using a Bruker WIN-EPR Software.

RT ^{13}C NMR measurements were carried out by a Tecmag LIBRA Pulse Solid State NMR/NQR spectrometer in an external magnetic field of 8.0196 T ($\nu_0 = 85.86$ MHz). The spectra were obtained by a spin echo Fourier Transform technique using a 16-phase cycling procedure. The $\pi/2$ pulse length was 5 μs and the repetition rate was about $5T_1$. The spin–lattice relaxation time T_1 was measured using a $\pi-\tau-\pi/2$ inversion recovery sequence. ^{13}C chemical shifts are given relative to tetramethylsilane (TMS), whose position is set to 0 ppm. For the measurements, we used liquid C_6H_6 ($\delta = +132$ ppm [16]) and pure C_{60} powder ($\delta = +143$ ppm [17]) as secondary references. Only the most contaminated initial UDD #1 sample and the 'purest' UDD #5 one (discussed later) were studied in detail.

The X-ray diffraction measurements were carried out on a Rigaku D-max RC diffractometer with copper radiation ($\lambda = 1.542$ Å), operating in reflection Θ–2Θ geometry. Equal amounts of UDD powder were used in all experiments, thus permitting a quantitative comparison of the scattered X-ray intensities. The HRTEM data were obtained by JEOL JEM-2010 operated at 200 keV.

3. Results

3.1. EPR

The RT EPR measurements were made on UDD samples ##1–5. Each sample was recorded under different experimental conditions. A large amount of the sample (~1 g), the scan width of 0.6 T, and a high receiver gain (RG) allowed detecting traces of transition metal ion impurities (Fig. 1). Here, the sharp signal at $g \sim 2.0$ is distorted. A narrow scan width of 30 mT and a low modulation amplitude were used for a precise recording of free-radical signals (Fig. 2). The EPR spectrum of the initial, detonation carbon (UDD #1) consists of two overlapping signals: an intense broad line at $g = 2.5$ and peak-to-peak line-width $\Delta H_{pp} \sim 170$ mT and a narrow line at $g \sim 2.0$ (here and further, see Fig. 1). The chemical treatment considerably reduced the broad line intensity. Thus, for #2 and #5 no broad signals were detected except for a very weak signal at $g = 4.25$ in UDD #5. Samples #3 and #4 show weak broad signals of another line shape and position.

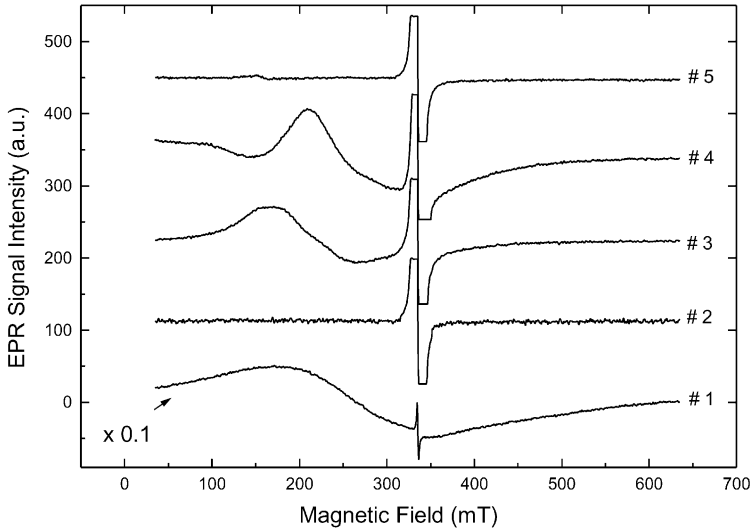

Fig. 1. A general view of the RT EPR spectra of UDD ##1–5, recorded from ~1 g of powders at RG = 10^5 (UDD #1) and RG = 10^6 (UDD ##2–5); $\nu = 9.38$ GHz.

The EPR spectra of narrow signals demonstrate the same Lorentzian line-shapes and g-factors of 2.0027 ± 0.0001 for all UDD samples (Fig. 2). The actual quantity of radical-type paramagnetic species was obtained by baseline correction and numerical double integration of the respective first-derivative EPR signal. This quantity is minimal for the detonation sample UDD #1 and corresponds to the concentration of these radical-like paramagnetic centers (RPCs) of 10^{19} spin/g. All purified samples ##2–5 show practically the same intense EPR signal, which corresponds to the RPCs concentration of 10^{20} spins/g. The line-widths vary among the samples as: $\Delta H_{pp}(\#1) = 1.25 \pm 0.01$ mT, $\Delta H_{pp}(\#2) = 0.81$ mT, $\Delta H_{pp}(\#3) = 0.84$ mT, $\Delta H_{pp}(\#4) = 0.75$ mT and $\Delta H_{pp}(\#5) = 0.97$ mT. No EPR saturation effect was reached for the narrow signals of all UDD samples up to microwave power of 200 mW—the maximum power available in our experimental set (Fig. 3). One can suggest, therefore, that the electron spin–lattice relaxation times are the same for all of the samples and are shorter than 10 μs. Aiming the elucidation of the effect of absorbed molecular oxygen on the RPC's lines, RT EPR spectra under in situ pumping (~10^{-4} Torr) were measured on the sample UDD #5. It was found that pumping abruptly increases the total amount of RPCs for about 10% (determined by spectra integration). No changes in the line shape, position and widths were detected. When pumping was

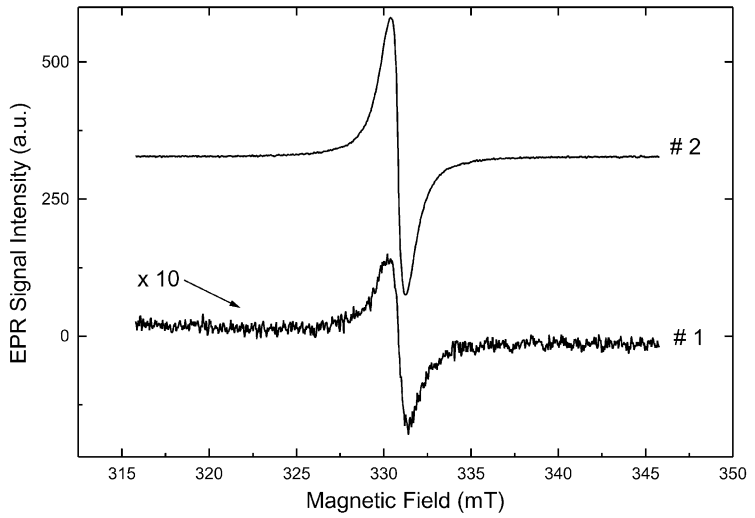

Fig. 2. The free-radical region in the RT EPR spectra of UDD #1 and #2. The spectra were recorded from the same amounts of powders (~200 mg) at RG = 10^6, $\nu = 9.268$ GHz (#1) and RG = 10^5, $\nu = 9.272$ GHz (#2).

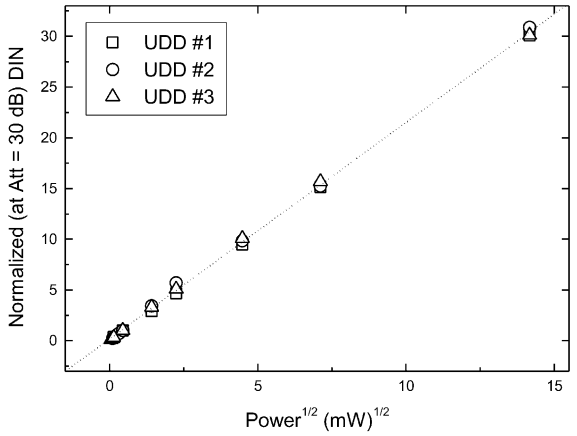

Fig. 3. Saturation curves for 3 UDD samples at RT. The intensities for each sample were normalized to the corresponding intensity of the spectra recorded at the incident power level of 200 μW.

stopped and the sample was open to air, the RPCs signal returns to its initial value.

A temperature-dependent EPR study of the narrow signal was made on the UDD #5 sample. The EPR spectra show a single Lorentzian line within the whole temperature range (4.2–300 K). The *g*-factor at RT is equal to 2.00282 ± 0.00003 and remains almost constant down to 4.2 K, the lowest temperature in our experiment (Fig. 4(a)). The line intensity obeys the Curie law (Fig. 4(b)).

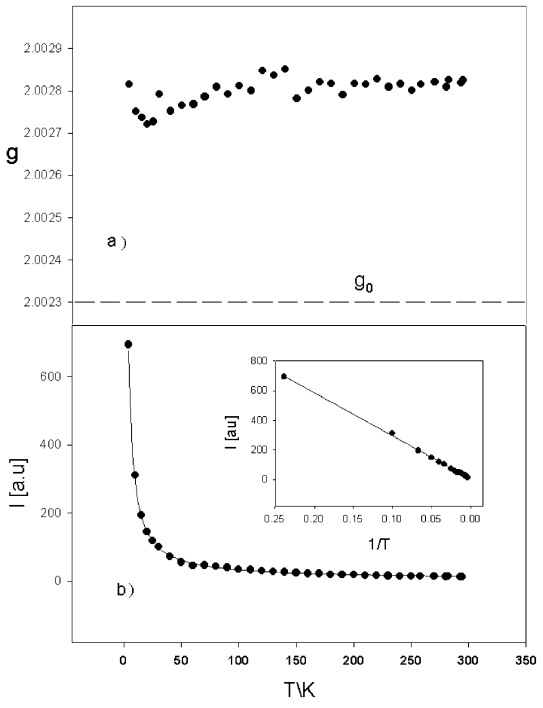

Fig. 4. Temperature-dependent EPR from UDD #5: (a) *g*-factor vs. temperature; (b) Curie-like behavior of the signal intensity.

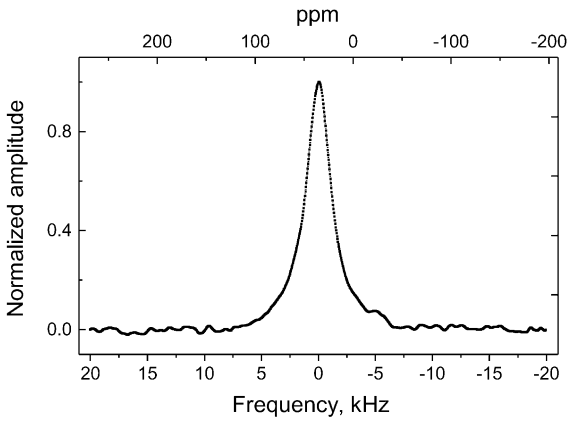

Fig. 5. The RT ^{13}C NMR spectrum of UDD #5.

3.2. ^{13}C NMR spectra and spin–lattice relaxation

The ^{13}C NMR spectrum of UDD #5 is shown in Fig. 5. It shows a single Lorentzian-like resonance with the linewidth $\Delta\nu = 2.1$ kHz and chemical shift $\delta = 35 \pm 3$ ppm relative to TMS, the latter coinciding with that of bulk diamond known from the literature (35 ppm, [16,18,19]). The ^{13}C NMR spectrum of UDD #1 (not shown) recorded at a slower repetition rate demonstrates a superposition of two lines belonging to disordered/turbostratic graphite and diamond, respectively. The intensity of the diamond-like line in that NMR spectrum is about 20 times lower than in the spectrum of #5.

The measurements of ^{13}C nuclear spin–lattice relaxation in UDD #5 show magnetization decay well described by a stretched exponent:

$$M(t) = M(0)\{1 - B\exp[-(t/T_1)^a]\} \quad (1)$$

with $T_1 = 144 \pm 10$ ms, $B = 1.91 \pm 0.04$, and $a = 0.661 \pm 0.027$ (Fig. 6). The relaxation time for the weak diamond-like line for sample #1, obtained by the same method, was found to be $T_1 = 173 \pm 45$ ms (here, the larger experimental error is due to a poor signal-to-noise ratio).

3.3. TEM characterization

Fig. 7(a) shows an electron micrograph of a detonation carbon sample before its purification. One can see compact rounded aggregation of disoriented fragments of graphene planes (black lines) with a characteristic size of 10–40 Å and an interplane distance of 3.4 Å close to those typical for crystalline graphite. This type of carbon is known as turbostratic carbon.

An electron micrograph of a UDD sample after an intense chemical purification is shown in Fig. 7(b). It is seen that

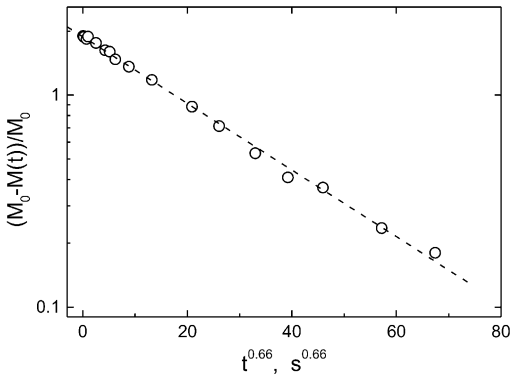

Fig. 6. The time dependence of ^{13}C magnetization decay for UDD #5 at RT.

there is practically no turbostratic carbon, while the crystalline diamond cores are clearly identifiable. The cluster cores are surrounded by a dark broken line. Such a pattern can be due to both edge effects producing smooth moire around the cluster and a shell consisting of graphene planes fragments. The structures shown by dark parallel lines correspond to the (111) diamond plane. The size of the quasi-spherical cores in the image plane varies between 40 and 60 Å. It follows from this image that the thickness of graphene shells does not exceed 4 Å, i.e. a single layer thickness.

Despite the clear difference in the small-angle X-ray scattering patterns (curves 5 and 6 in Fig. 8), the TEM images show no difference in the shell structure of UDD clusters produced by dry and wet syntheses.

4. Discussion

Let us first analyze the EPR data. The broad intense line observed in the EPR spectrum of the initial UDD #1 sample clearly indicates the presence of a certain amount of EPR active species unrelated to structural defects in both graphite and diamond. Since corresponding lines are broad and structureless, no precise data on their origin are available. However, such lines are typical for samples, which contain both paramagnetic and ferromagnetic impurities originating from transition metal ions such as Fe^{3+}, Cr^{3+}, Mn^{2+}, Co^{2+}, Ni^{2+} and Cu^{2+}. The EPR spectra of the UDD samples which undergo chemical treatment (##2–5) show a significant reduction in the amount of magnetic impurities. Moreover, these EPR spectra provide information on the efficacy of the chemical treatment procedure. Thus, the most 'free from magnetic ions' sample is #2. Samples #3 and #4 still contains detectable amount of impurities. Sample #5 contains just a negligible amount of rhombically distorted Fe^{3+} complexes responsible for the weak line at $g \sim 4.3$.

These EPR data are supported by the X-ray diffraction patterns for the samples subjected to different chemical purifications (Fig. 8). Indeed, the diffraction pattern of detonation carbon (curve 1) contains both broad diffraction maxima, related to the scattering by nanodiamonds and nanographite particles, and a series of narrow maxima corresponding to diffraction by large inclusions of magnetite ($FeFe_20_4$). The chemical extraction removes both nanocrystalline graphite and large crystal impurities, detectable by X-ray techniques (curves 4–5). Simultaneously, a halo at $2\theta_{Br} \sim 17°$ appears in the samples produced by both dry (curve 4) and wet (curve 5) syntheses following the chemical etching. The halo at ca. $2\theta_{Br} \sim 15–18°$ is sometimes observed in natural carbon and attributed with steaks of two to four graphene layers [20]. We attribute the 17° halo to the diffuse scattering by sets of equidistant nanosized graphene plates distributed randomly on the onion-like

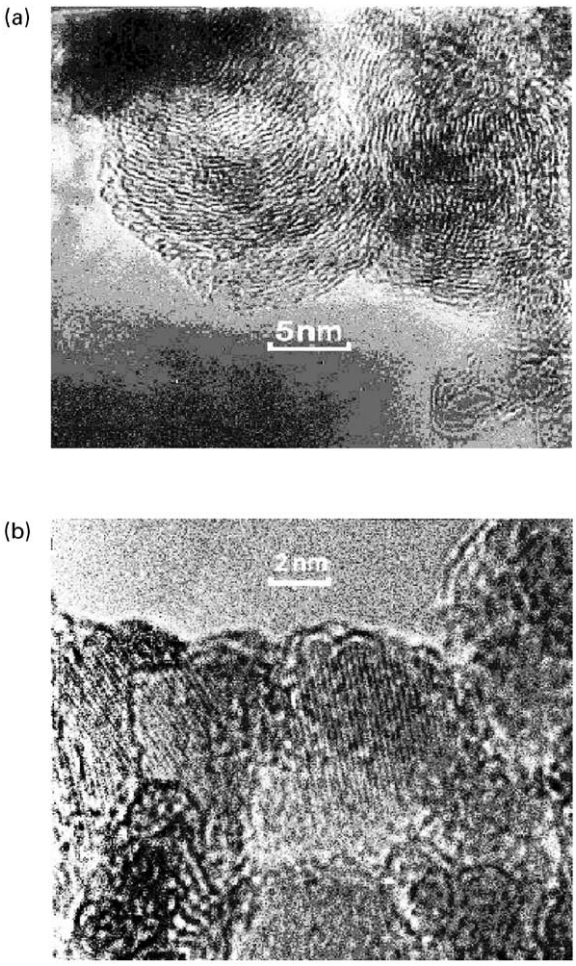

Fig. 7. The HR TEM images illustrating the effect of chemical purification of detonation carbon: (a) detonation carbon, (b) ultradisperse diamond particles after the treatment of detonation carbon (#6). The distance between layers of the onion-like carbon shell is ca. 0.35 nm (a). The diamond lattice of the UDD core is clearly seen (b).

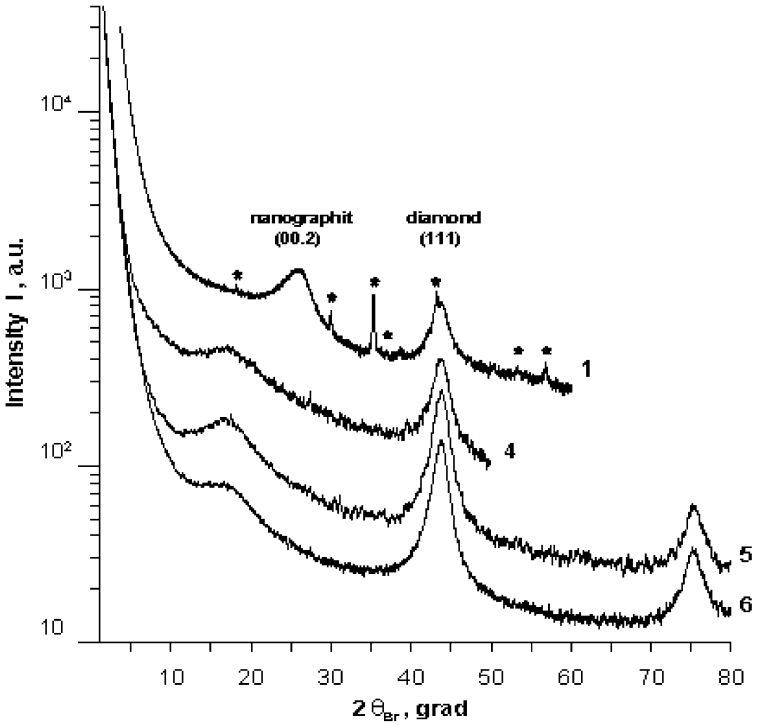

Fig. 8. The diffraction pattern of UDD samples differing in the extent of purification. The etching parameters are given in Table 1 (the sample numbers coincide with the numbers of the entries. The asterisks indicates the $FeFe_20_4$ diffraction maxima (JCPDS file #19-0629).

shell surrounding the diamond core [15]. In the case of turbostratic stacking of graphene layers (or carbon black) a broad diffraction peak at ca. $2\theta_{Br} \sim 26°$ has been observed (similar to our case of detonation carbon, see Fig. 7(a), and curve 1 in Fig. 8).

Since the thickness and structure of a shell depend on the kinetics of its formation, the halo intensities differ noticeably (compare the curves 5 and 6); an analysis of the effect was shown earlier in Ref. [15]. Note that the diffraction patterns from #2 to #6 are similar to curve 5 in Fig. 8.

A narrow Lorentzian-like signal with $g \sim 2.003$ and $\Delta H_{pp} \sim 1$ mT was previously reported for nanodiamonds by several research groups [21–23]. The RT EPR parameters of this signal (the g-value, ΔH_{pp} and electron spin–lattice relaxation time) are in a good agreement with the values reported in Ref. [22] ($g = 2.0028$ and $\Delta H_{pp} \sim 1$ mT for samples heat-treated below 1600 °C) and Ref. [22] ($g = 2.003$ and $\Delta H_{pp} = 0.96$ mT for the wet synthesis). The RPCs, responsible for these signals, are commonly identified as carbon-inherited localized Curie spins [22]. In accordance with the results in Ref. [23], no nitrogen-related RPCs were detected and no Pauli paramagnetic term from the conducting nanographite π-electron network was found. The pure Curie-like behavior in the low temperature range (Fig. 4(b)) confirms the localized character of those RPCs. It also indicates that no diamond-to-graphite conversion due to the chemical treatment occurred in the present experiment. The concentration of localized spins in purified UDD samples, obtained from the EPR data (10^{20} spin/g), is in a perfect agreement with that value calculated in Ref. [22] from the Curie constants.

The question on the origin of localized carbon-inherited RPCs is of paramount importance. There are several reasons to believe that these RPCs are due to dangling bonds associated with structural defects on the diamond core of the cluster, i.e. with sp^3-hybridized carbon rather than with turbostratic disordered carbon. The key experimental fact, which must be explained in the discussion on RPCs origin, is the significant increase in their concentration with increasing efficacy of the detonation carbon purification. Note first that the measurement of the diamond fraction has shown that the detonation carbon, produced by the dry synthesis, contains about 35% of diamond and that of the wet synthesis contains 70%. This means that the same, an order of magnitude higher concentration of RPCs (10^{20} instead of 10^{19} spin/g), observed in all purified samples is absolutely inconsistent with a larger diamond fraction in the initial sample. Since the chemical treatment affects only the cluster surface, the change in RPCs concentration may be considered to be due to this fact. In the model offered in Ref. [15], the UDD nanocrystal is covered by a shell consisting of one or several graphene layers, depending on the purification intensity. These layers arise from the partial diamond–graphite transition at the final stage of

the detonation synthesis. Following a shock wave, the pressure becomes too low for the thermodynamic diamond stability to persist, while the temperature remains high. The existence of such a shell is indicated by the SAXS data on UDD samples [14]. Cluster shells of thickness greater than 3–4 atomic layers can be clearly seen in TEM images. They are known as onion-like structures and can be produced by UDD heat treatment [8,11] and even by the intense electron irradiation in TEM studies [10].

An indirect evidence for a residual fraction of sp^2-hybridized carbon after chemical treatment is the color of powder-like UDD samples, which varies from nearly black to light gray, depending on the purification intensity. It is quite likely that the closed structure and the strong bonding of the shell to the diamond core prevent its complete removal. The UDD samples studied had a shell of 1–2 atomic layers after the chemical treatment. A shell of this thickness can be hardly observed in high-resolution TEM images.

The periodic structure of parallel lines in the image of Fig. 7(b) corresponds to the (111) diamond plane. The size of a single crystal cluster core, evaluated from the interplane distance of 2.05 Å for bulk diamond, has been found to be 45 Å, in agreement with earlier data [6,8,15]. It is the graphene cluster shell, which seems to contain defects like unpaired valence electrons observed as RPCs. These defects might be attributed to the edges and breaks of the graphene planes. On the other hand, judging from the UDD structure prior to the chemical treatment (Fig. 8(a)), the content of graphene plane fragments in the sample is much higher than after the treatment. The image scale can be found from the step of the quasi-parallel bands, which correspond to mismatched graphene planes with a typical interplane distance of 3.4 Å. Therefore, RPCs cannot be quantitatively associated with the plane edges. The local concentration of RPCs in purified samples ##2–5, estimated from the average UDD density of about 3 g/cm^3 [4], was found to be only 10 spins per cluster, regardless of the techniques used for the synthesis and purification. The amount of surface atoms per a diamond core in a cluster of 45 Å in size (when the unit cell in bulk diamond is 3.55 Å and the number of atoms per cell is $n = 8$) is found to be about 2400 for a spherical cluster and 2100 for an octahedral one. The comparison of these values with the earlier estimated amount of RPCs per cluster leads one to the conclusion on a small number of dangling bonds per UDD cluster, in spite of their total high content in the sample. This is an additional evidence for a large amount of surface atoms relative to bulk atoms, which is characteristic of cluster substances.

One can draw the conclusion from the foregoing discussion that the surface bonds of a diamond core are nearly totally terminated, and the observable RPCs must be due to structural defects at the interface between the core and the first graphene layer of the cluster shell.

Another argument in favor of attributing the localized spin EPR signals to the UDD diamond core follows from the analysis of the g-factor. All g-values reported for nanodiamond samples [21–23] are close to the g-value of pulverized colorless diamond, in which the spins are attributed to RPCs created by defects in the sp^3-bonded network ($g = 2.0027 \pm 0.0002$) [24]. We found experimentally the same g-value for the narrow signal from UDD samples, using two independent techniques. Moreover, the measurement with a tracking field/frequency calibration allowed us to reduce the experimental error by about an order of magnitude and to get a more precise value of $g = 2.00282 \pm 0.00003$.

Two effects may change the electronic properties of small particles in a nanometer material, as compared with those of a bulk material—the surface effects and quantum-size effects [25,26]. For example, the conduction electron spin resonance will differ for small particles and a bulk material. This is due to a discrete structure of the energy levels in nanoparticles. The size dependence of the g-factor in small particles was discussed by Butter et al. [24], Kawabata [26] and Myles [27]. These authors have shown that the particle size strongly influences the g-factor value on a nanometer scale. A general conclusion from Refs. [25,27] (in contradiction with Ref. [26]) is that the absolute g-shift ($\Delta g = g - g_0$, where $g_0 = 2.0023$) should decrease with decreasing particle size. The size-dependent contribution to the g-shift, $\Delta g(L)$, is independent of the particle shape and may be written as [25,27]

$$\Delta g(L) = [1 - \alpha(c/L)]\Delta g(\infty), \tag{2}$$

where L is the edge length of a cubic box or the radius of a spherical particle, c the lattice constant, α a parameter of the order of unity, and $\Delta g(\infty)$ is the g-shift of the bulk material. Eq. (2) (slightly modified) was used by Stankowski et al. [28] to describe RPCs localized on the C_{60} molecule which may also be treated as a mesoscopic object. We have postulated that the signal observed in UDD is a carbon-inherited RPCs of a hole origin with $g > g_0$ [23]. Here, we can use Eq. (2) to estimate the size of diamond nanoparticles of UDD #5. All of g-factors, found for carbon-related defects in various diamond samples (both films and a bulk diamond in the crystalline and amorphous phases [29–35]) coincide, within the experimental error of 2×10^{-4}, with the same value of 2.0029. Thus, the g-shift for a bulk material $\Delta g(\infty)$ may be suggested to be equal to 6×10^{-4}. The size-dependent g-shift for small particles from the present experiment is equal to $\Delta g(L) = (5.2 \pm 0.3) \times 10^{-4}$. Taking the lattice constant to be $c = 3.573$ Å, which is measured for a particular sample and is characteristic for UDD, one can find from Eq. (2) the average diameter of the UDD particles varying (due to the experimental error) from 20 to 45 Å. This estimation is in a good agreement with those reported for nanodiamond materials produced by a similar method [21–23], as well as with our present HR TEM data (see Fig. 7(b)).

As it was pointed out in Ref. [22], the line-width of EPR signals from carbon-inherited RPCs in UDD is dependent on the way the synthesis carried out. The maximum line-width

was found for the detonation soot sample #1 to be $\Delta H_{pp} = 1.25$ mT. The main reason for the line broadening here may be the interaction with ferro- and paramagnetic impurities detected in this sample by EPR. UDD ##2–4 obtained by dry syntheses demonstrates narrow EPR lines of practically the same line-width of about 0.8 mT. Sample #5 produced by the wet synthesis shows a broader line with $\Delta H_{pp} = 0.97$ mT. Since the concentration of RPCs for the samples obtained by the two syntheses methods was found to be the same, this difference suggests that no spin–spin interaction is responsible for the line broadening in the sample obtained by the dry synthesis. Contrary to Ref. [23], however, we cannot exclude the spin–nuclear interaction of the carbon-inherited paramagnetic defect with neighboring hydrogens, as was found for CVD diamond films by both EPR and ENDOR [31]. The pumping experiment shows that the interaction with absorbed molecular oxygen does not affect the line-width of the RPCs observed. On the other hand, 10% increase of the actual amount of observable RPCs may be explained just by the dipolar interaction of RPC with paramagnetic O_2. Indeed, in the non-pumped sample some RPCs are located in the close vicinity of oxygen molecules. Dipolar interaction causes significant broadening of EPR lines for these RPCs, which reduces their contribution to the observed signal integrated within the limiting field range. When pumping proceeds, the line-widths of these RPCs narrow and they contribute to the integral again. Detailed EPR study of the oxygen–RPCs interaction lies outside the scope of the present article and will be reported elsewhere.

We will now analyze the NMR data. A diamond crystal is diluted in magnetic nuclei because of the low natural abundance of ^{13}C isotope, 1.1%, which yields negligible dipole–dipole interactions of the nuclei. The cubic structure of diamond must produce an isotropic chemical shift. Moreover, UDD #5 practically exhibits no magnetic impurity particles. Therefore, it is expected to show a reasonably narrow nuclear resonance line with a width that should be comparable with the instrumental broadening (about 100 Hz). However, the width of the observed NMR signal is 2.1 kHz. To explain such a line-width, we must keep in mind that nanoparticles usually show a behavior quite different from that of bulk material. The latter occurs due to the significant contribution of surface atoms, whose amount, in our case, is comparable with that of the bulk region. In the case under consideration, one can suggest that the surface has a structure distorted relative to the 'bulk' diamond structure. Thus, each magnetic nucleus 'senses' different electronic environments causing a distribution of the chemical shifts of NMR frequencies of carbon atoms, which manifests itself in a line broadening. Such a broadening is usually observed in the NMR spectra of nanosized particles [36–40]. Recent ab initio calculations of ^{13}C NMR chemical shifts of a diamond surface have predicted that atomic layers lying close to the surface experience strong variations in the chemical shift [41].

The stretched exponential time dependence of the magnetization decay $M(t)$ was obtained by ^{13}C nuclear spin–lattice relaxation measurements of the UDD #5 sample, which exhibits practically no magnetic impurities and the highest degree of removal of the non-diamond phase. Such a stretched exponential dependence of $M(t)$ is the classic behavior characteristic of the nuclear spin–lattice relaxation via RPCs [42], where coefficient α in Eq. (1) is equal to $D/6$ or $(D + d)/6$ for uniform and non-uniform distributions of RPCs and nuclei, respectively [43]; here D is the space dimensionality of the sample and d is the dimensionality of the nuclear magnetization space. Three-dimensional structure of diamond yields $D = 3$. In the high field NMR experiment, since the spin magnetization is confined to the direction of the external magnetic field, the dimensionality of the nuclear magnetization space $d = 1$. Thus $\alpha = (D + d)/6 = 0.66$, that is in an excellent agreement with our experimental data.

We would like to emphasize that available data on ^{13}C spin–lattice relaxation in natural diamond and some synthetic diamonds show very long values of T_1, which vary from one to several hours [18,44–46]. This is mainly due to the low natural abundance of ^{13}C isotope, the absence of chemical shielding anisotropy, and the diamond lattice rigidity. However, the spin–relaxation time of the UDD #5 sample, $T_1 = 144 \pm 10$ ms, is almost three orders of magnitude shorter than that reported in literature. We have noted that the UDD #5 sample shows practically no magnetic impurities and the highest degree of the removal of the non-diamond phase; moreover, any impurity, mechanically separated from the diamond core, does not affect the nuclear relaxation. Thus, the dramatic change in T_1 is readily due to the large amount of RPCs detected by EPR. It has been mentioned that the structural model of these RPCs is a broken, dangling C–C bond at the interface between the core and the first graphene layer of the cluster shell, yielding a localized unpaired electron. The coupling between nuclear spins and unpaired electron spins, even in small concentrations, creates an effective channel for the nuclear spin–lattice relaxation [47]. Therefore, one can conclude that the only mechanism that can lead to such a high relaxation rate is the nuclear relaxation via the localized electron spins.

The strong influence of RPCs on the ^{13}C spin–lattice relaxation rate means that both RPCs and ^{13}C nuclei of diamond are likely to be localized in the same 'lattice'. This model is also supported by practically the same relaxation times for samples #1 and #5, which means that numerous graphite inclusions in UDD #1 (as well as external magnetic impurities) practically have no effect on T_1 of nanocrystalline diamonds. Note that the graphite component in UDD #1 shows a fairly long relaxation time (several tens of seconds), which is characteristic for graphite and is too far from the value obtained for the nanodiamond.

5. Summary

The EPR and ^{13}C NMR studies on detonation carbon and

ultradisperse diamond clusters, together with available X-ray diffraction and TEM data, have shown that a high concentration of paramagnetic centers (up to 10^{20} spin/g) is due to structural defects (dangling C–C bonds) on the diamond cluster core. It is found that the defects are localized on the cluster surface. We have detected a variation in the *g*-factor of the unpaired electron associated with the size-effect.

The anomalous reduction in the spin–lattice relaxation time of ^{13}C (from several hours in natural diamond to ~150 milliseconds in UDD clusters), as well as stretched exponential character of the magnetization decay, is attributed to the interaction between the unpaired electrons of RPCs and nuclear spins. It has been demonstrated that the EPR technique can be successfully used for the estimation of UDD purification.

Acknowledgements

The Ioffe Institute authors acknowledge support under the Russian State Program 'Fullerenes and Atomic Clusters'.

References

[1] A.M. Staver, N.V. Gubareva, A.I. Lyamkin, E.A. Petrov, Physica Goreniya i Vzryva 20 (1984) 100 in Russian.
[2] N.R. Greiner, D.S. Phillips, J.D. Johnson, F. Volk, Nature 333 (1988) 440.
[3] V.I. Trefilov, V.S. Moskalenko, G.I. Savvakin, E.A. Tsapko, D.G. Savvakin, Dok. Akad. Nauk SSSR 305 (1989) 85 in Russian.
[4] V.L. Kuznetsov, A.L. Chuvilin, E.M. Moroz, V.N. Kolomiichuk, S.K. Shaikhutdinov, Y.V. Butenko, Carbon 32 (1994) 873.
[5] M. Yoshikawa, Y. Mori, H. Obata, M. Maegawa, G. Katagiri, H. Ishida, A. Ishitani, Appl. Phys. Lett. 67 (1995) 694.
[6] A.E. Alexenskii, M.V. Baidakova, Phys. Solid State 39 (1997) 1037.
[7] H. Makuta, K. Nishimura, N. Jiang, A. Hatta, T. Ito, A. Hiraki, Thin Solid Films 281–282 (1996) 279.
[8] V.L. Kuznetsov, A.L. Chuvilin, Y.V. Butenko, I.Yu. Malkov, V.M. Titov, Chem. Phys. Lett. 222 (1994) 343.
[9] E.D. Obraztsova, M. Fujii, S. Hayashi, V.L. Kuznetsov, Y.V. Butenko, Carbon 36 (1998) 821.
[10] F. Banhart, P.M. Ajayan, Nature (1996) 382.
[11] S. Tomita, M. Fujii, S. Hayashi, K. Yamamoto, Diamond Relat. Mater. 9 (2000) 856.
[12] P. Badziak, W.S. Verwoerd, W.P. Ellis, N.R. Greiner, Nature 343 (1990) 244.
[13] M.Y. Gamarnik, Phys. Rev. B 54 (1996) 2150.
[14] M.V. Baidakova, A.Ya. Vul', V.I. Siklitski, Chaos, Solitons Fractals 10 (1999) 2153.
[15] A.E. Alexensky, M.V. Baidakova, A.Ya. Vul', V.I. Siklitski, Phys. Solid State 41 (1999) 669.
[16] T.M. Duncan, J. Phys. Chem. Ref. Data 16 (1987) 125.
[17] R. Tycko, G. Dabbagh, R.M. Fleming, R.C. Haddon, A.V. Makhija, S.M. Zahurak, Phys. Rev. Lett. 67 (1991) 1886.
[18] M.J. Duijvestijn, C. van der Lugt, J. Smidt, R.A. Wind, K.W. Zilm, D.C. Staplin, Chem. Phys. Lett. 102 (1983) 25.
[19] H.L. Retcofsky, R.A. Friedel, J. Phys. Chem. 77 (1973) 68.
[20] V.V. Kovalevski, P.R. Buseck, J.M. Cowley, Carbon 39 (2001) 243.
[21] O.E. Anderson, B.L.V. Prasad, H. Sato, T. Enoki, Y. Hishiyama, Y. Kaburagi, M. Yoshikawa, S. Bandow, Phys. Rev. B 58 (1998) 16387.
[22] B.L.V. Prasad, H. Sato, T. Enoki, Y. Hishiyama, Y. Kaburagi, A.M. Rao, P.C. Eklund, K. Oshida, M. Endo, Phys. Rev. B 62 (2000) 11209.
[23] K. Iakoubovskii, M.V. Baidakova, B.H. Wouters, A. Stesmans, G.J. Adriaensens, A.Ya. Vul', P.J. Grobet, Diamond Relat. Mater. 9 (2000) 861.
[24] G.K. Walters, T.L. Estle, J. Appl. Phys. 32 (1961) 1854.
[25] J. Butter, R. Car, Ch.W. Myles, Phys. Rev. B 26 (1982) 2414.
[26] A. Kawabata, J. Phys. Soc. Jpn 29 (1970) 902.
[27] Ch.W. Myles, Phys. Rev. B 26 (1982) 2648.
[28] J. Stankowski, L. Piekara-Sady, W. Kempiński, Appl. Magn. Res. 19 (2000) 1.
[29] M. Fanciulli, T.D. Moustakas, Physica B 185 (1993) 228.
[30] M. Fanciulli, T.D. Moustakas, Phys. Rev. B 48 (1993) 14982.
[31] D.F. Talbot-Ponsonby, M.E. Newton, J.M. Baker, G.A. Scarsbrook, R.S. Sussmann, A.J. Whitehead, S. Pfenninger, Phys. Rev. B 57 (1998) 2264.
[32] Y. Show, M. Iwase, T. Izumi, Diamond for electronic applications, Symp. Mater. Res. Soc., Pittsburgh, PA, USA XII + (1996) 169.
[33] C.F.O. Graeff, E. Rohrer, C.E. Nebel, M. Stutzmann, H. Guttler, R. Zachai, III-nitride SiC and diamond materials for electronic devices, Symp. Mater. Res. Soc., Pittsburgh, PA, USA XVII + (1996) 495.
[34] C.F.O. Graeff, C.E. Nebel, M. Stutzmann, Braz. J. Phys. 27A (1997) 68.
[35] N. Casanova, E. Gheeraert, A. Deneuville, C. Uzan-Saguy, R. Kalish, Phys. Stat. Sol. (a) 181 (2000) 5.
[36] A.M. Thayer, M.L. Steigerwald, T.M. Guncan, D.C. Douglass, Phys. Rev. Lett. 60 (1988) 2673.
[37] K. Kimura, Phase Transitions 24–26 (1990) 493.
[38] J.J. van der Klink, H.B. Brom, Prog. Nucl. Magn. Reson. Spectrosc. 36 (2000) 89.
[39] K.M. McNamara, K.K. Gleason, D.J. Vestyck, J.E. Butler, Diamond Relat. Mater. 1 (1992) 1145.
[40] J.H. Strange, Proceedings of the 30th Congress AMPERE on Magnetic Resonance and Related Phenomena, Lisbon, Portugal, 2000.
[41] F. Mauri, B.G. Pfrommer, S.G. Louie, Phys. Rev. B 60 (1999) 2941.
[42] W.E. Blumberg, Phys. Rev. 119 (1960) 79.
[43] G.B. Furman, E.M. Kunoff, S.D. Goren, V. Pasquier, D. Tinet, Phys. Rev. B 52 (1996) 10182.
[44] M.J.R. Hoch, E.C. Reynhardt, Phys. Rev. B 37 (1988) 9222.
[45] E.C. Reynhardt, C.J. Terblanche, Chem. Phys. Lett. 269 (1997) 464.
[46] C.J. Terblanche, E.C. Reynhardt, J.A. van Wyk, Chem. Phys. Lett. 310 (1999) 97.
[47] A. Abragam, The Principles of Nuclear Magnetism, Oxford University Press, Oxford, 1961.